Wavelength scaling and multicolor operation of a plasma-driven attosecond x-ray source via harmonic generation

Rafi Hessami,[1,*] Jenny Morgan,[1,†] River Robles,[1,‡] Kirk A. Larsen,[1,2,§] Agostino Marinelli,[1,‖] and Claudio Emma[1,¶]

[1]*SLAC National Accelerator Laboratory, Menlo Park, California, USA*
[2]*Stanford PULSE Institute, Stanford, California, USA*

(Received 1 January 2024; accepted 20 June 2024; published 12 July 2024)

The generation of high-power coherent soft x-ray pulses of sub-100 as duration and 10 nm wavelength using beams from a GeV energy plasma wakefield accelerator has been recently investigated in Emma *et al.* [APL Photonics **6**, 076107 (2021)]. As a future upgrade to this concept, this contribution investigates scaling to shorter x-ray wavelengths by cascading undulators tuned to higher harmonics of the fundamental. We present two simulation studies for plasma-driven attosecond harmonic generation schemes with final photon wavelengths of 2 and 0.40 nm. We demonstrate in these schemes that using undulators with retuned fundamental frequencies can produce GW-scale pulses of sub-nm radiation with tens of attosecond-scale pulse lengths, an order of magnitude shorter than current state-of-the-art attosecond x-ray free electron lasers (XFELs). This multipulse multicolor operation will be broadly applicable to attosecond pump-probe experiments.

DOI: 10.1103/PhysRevAccelBeams.27.070701

I. INTRODUCTION

X-ray free electron lasers (XFELs) are powerful scientific instruments that enable the exploration of natural phenomena down to attosecond timescales and Angstrom spatial scales [1]. State-of-the-art attosecond XFELs are able to produce x-ray beams with 100 μJ-scale pulse energies with measured pulse lengths down to 280 as at nm-wavelengths [2–4]. Single-spike hard x-ray operation has also been demonstrated with estimated pulse durations in the hundreds of attoseconds [5–7]. Reaching sub-100-as timescale has interesting ramifications for studying ultrafast electronic phenomena, such as allowing the study of molecular relaxation and charge redistribution following the sudden removal of an electron, or improving the fidelity of attosecond pump/probe experiments for the observation of charge migration in molecules [8,9]. To reach the sub-100 as regime, a recent paper has proposed using beams from plasma wakefield accelerators compressed to an ultrashort bunch length (22.3 nm FWHM) to generate sub-100 as TW-scale pulses at 10 nm wavelength [10]. The working principle of this plasma-driven scheme takes advantage of the compressed beam's high peak current and natural bunching factor at tens of nanometers to reach saturation in an ultrashort m-length undulator [11–13].

Harmonic up-conversion for FEL lasing has been demonstrated in Ref. [14] using an external laser seed. Additional harmonic seeding methods include variations of high-gain harmonic generation (HGHG) [15,16] and echo-enabled harmonic generation (EEHG) [17–20]. Experiments with EEHG have shown that pulses at 5.9 nm with an FWHM between 130 and 175 fs can be generated using this technique [20]. In this paper, we show that combining a plasma-driven attosecond x-ray source with a harmonic generation scheme enables the production of high-power (GW scale), sub-100-as x-ray pulses at wavelengths down to the sub-nm level with a 3.3 GeV energy electron bunch in an ultracompact (m-length) undulator. A scheme to produce attosecond-angstrom pulses using the beam quality advantages of a plasma photocathode has been proposed elsewhere [21]. Additional proposed methods include using a seeded FEL to ensure isolated bunching in the middle of the beam, producing an attosecond pulse [22].

The method described in Ref. [10] can be extended to shorter wavelengths using a variation of the HGHG scheme, where the initial seed is provided by the coherent radiation generated by the nm-scale electron bunch from the plasma accelerator. In the harmonic generation scheme presented, the first undulator is used to generate radiation at the fundamental wavelength while simultaneously increasing

*Contact author: rafimah@stanford.edu
†Contact author: jmorgan@slac.stanford.edu
‡Contact author: riverr@stanford.edu
§Contact author: larsenk@stanford.edu
‖Contact author: marinelli@stanford.edu
¶Contact author: cemma@slac.stanford.edu

the beam's bunching factor at higher harmonics. Following this initial section, the harmonic bunching is exploited in one or more downstream undulators to generate short wavelength radiation with a prebunched beam. Additionally, since these beams are prebunched and the current spike in the beam is attosecond scale, the produced x-ray beams are also attosecond scale. In particular, this work presents two simulation studies: a harmonic generation configuration where the fundamental is tuned to 10 nm and the fifth harmonic at 2 nm is utilized and another configuration where the fundamental is tuned to 2 nm and the fifth harmonic at 0.40 nm is utilized. Since the fifth harmonic is at 2 nm, which lies beyond the carbon, nitrogen, and oxygen K edges, this scheme may provide utility for probing a multitude of chemical and biological systems.

A. Theoretical background

Typical FEL operation relies on the self-amplified spontaneous emission (SASE) process to generate radiation [23]. The minimum pulse length at saturation in the SASE process is set by the FEL cooperation length $L_c = \lambda/4\sqrt{3}\pi\rho$ where λ is the desired photon wavelength and ρ is the FEL parameter, typically $\mathcal{O}(10^{-4}$–$10^{-3})$ at x-ray wavelengths [23]. This parameter is given by $\rho = (\frac{1}{4}K(\gamma/\gamma_R)^2\Omega_P/\omega_u)^{2/3}$, where K is the undulator parameter, itself given by $K = \frac{eB\lambda_u}{2\pi m_e c}$, Ω_P is the relativistic plasma frequency, ω_u is the undulator frequency, and γ_R is the resonant energy, given by $\gamma_R^2 = \frac{\lambda_u(1+K^2)}{2\lambda_r}$, where λ_r is the resonant wavelength of the undulator [24,25]. This minimum pulse length, much longer than the photon wavelength, can be made shorter by increasing the magnitude of the FEL parameter using a high current spike to drive the FEL process. This was originally proposed in a scheme known as enhanced SASE in Ref. [26]. The original enhanced SASE scheme relies on using an external laser to chirp the beam before a weak bunch compression stage transforms the energy chirp into a large current spike at the compressor exit. It was also shown that in an enhanced SASE experiment, longitudinal space-charge forces play a crucial role in reshaping the phase space of the lasing spike [27], leading to the generation of pulses significantly shorter than the cooperation length [2,28] Recent experimental efforts have demonstrated this concept [3] and variations of this idea [2,4] to successfully generate 100-as-scale duration XFEL pulses at nm wavelengths.

Scaling this approach to shorter pulse duration using a plasma accelerator was proposed in Ref. [10]. The plasma-driven approach takes advantage of the high-brightness beams with naturally strong energy chirps produced in plasma accelerators, which can be compressed in a weak downstream chicane to extreme, near-MA peak currents and ultrashort 10-nm-scale bunch lengths. While this approach is successful at generating high-power attosecond pulses at the 10 nm wavelength level, the pulse energy drops significantly when lasing directly at wavelengths in the nm range, limited by the reduction in the beam's bunching factor at shorter wavelengths at the entrance to the undulator. Figure 1 demonstrates how the x-ray pulse energy and pulse duration generated by directly sending the compressed beam from a plasma-based accelerator into an undulator decreases as the wavelength shortens (see Table I for simulation parameters, the beam is identical to that used in [10]). This is expected, due to the reduced bunching factor and increased sensitivity to 3D effects such as

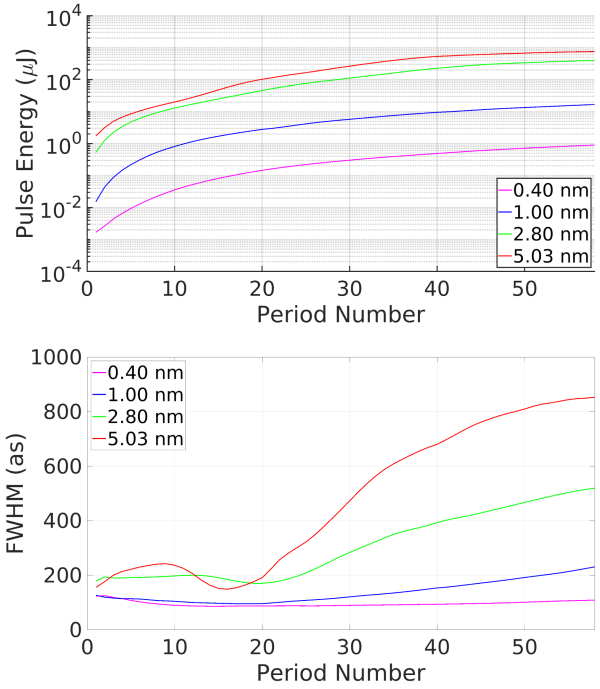

FIG. 1. X-ray pulse energy and pulse length from simulations along the undulator at different resonant wavelengths showing a decline in pulse energy and an increase in saturation length as the resonant wavelength is scaled down toward 0.40 nm. The decline in pulse energy and generation of pulse lengths consistently over 100 as at shorter x-ray wavelength motivates the use of the harmonic generation scheme to scale a plasma-based attosecond x-ray source into nm wavelengths while maintaining sub-100-as pulse duration. The beam parameters are given in Table II and are based on PUFFIN simulations for different undulator configurations using the beam from Ref. [10].

TABLE I. Simulation parameters for a single undulator tuned to successively reach shorter resonant wavelengths in a plasma-driven attosecond XFEL. The 0.40 nm simulation has a different undulator period because it was not possible to reach such a short resonant wavelength without changing the undulator period.

Resonant wavelength (nm)	K value	Undulator period (cm)
0.40	0.315	3.00
1.00	0.980	5.60
2.80	2.510	5.60
5.03	3.600	5.60

TABLE II. Electron beam parameters used in Ref. [10] and in the simulations presented in this paper.

Electron beam parameter	Value
Beam energy	3.28 GeV
Peak current	0.714 MA
Current spike width	22.3 nm FWHM

emittance and energy spread at shorter wavelengths. In particular, Fig. 1 shows that the x-ray pulse energy drops by 3 orders of magnitude when scaling from 5.03 to 0.40 nm wavelength. Concurrently, the minimum pulse length in this wavelength region is limited to 100 as or more.

Motivated by these considerations, in this work, we investigate using a harmonic-based approach to generate sub-100-as x-ray pulses with a plasma-based attosecond XFEL. The beam is initially transported through a first undulator section tuned to a subharmonic of the desired output wavelength, generating radiation at the subharmonic while increasing the bunching at higher harmonics. Following the first section, the prebunched beam is transported into one or more downstream undulators tuned to the desired wavelengths. This results in the emission/generation of a two-color attosecond x-ray pulse pair with GW power. In the following sections, we discuss the two schemes using the same electron beam input parameters at the start of each of the two configurations as used in the single-stage simulations.

II. HARMONIC GENERATION SIMULATIONS FOR A PLASMA-DRIVEN ATTOSECOND XFEL

The electron beam used in the harmonic generation simulations is the fully compressed attosecond duration bunch described in Ref. [10] and obtained from Particle-In-Cell simulations of the plasma wakefield acceleration process along with beam dynamics simulations of the bunch compression stage following the plasma accelerator. The notable properties of this electron bunch are the extremely high peak current (0.714 MA) and ultrashort bunch duration at the current spike (22.3 nm FWHM) which result in a substantial (% level) fraction of prebunching at wavelengths down to 10 nm. Additionally, the beam has an energy of 3.28 GeV.

The FEL simulations using the electron beam as input are performed using the FEL code PUFFIN [29]. This FEL code is well suited for simulating multicolor FEL operation as well as FELs that use ultrashort beams on the order of an FEL cooperation length [30] due to the fact that the code does not employ the slowly varying envelope approximation (SVEA) nor the period averaging approximation. In addition, to simulate very high peak current beams such as the one considered in this work, the code has been modified to include the effects of longitudinal space charge (LSC) which introduce non-negligible dynamics and affect of the beam distribution during its traversal in the undulator primarily through the generation of strong energy chirps in the longitudinal phase space. These chirps have known impacts on attosecond XFELs and are responsible for, among other factors, the shortening of the FEL pulse duration at saturation at the cost of reduced peak power [28].

A. 2 nm simulation

The first harmonic generation scheme we consider is a two-stage undulator setup in which the first undulator is tuned to the fundamental at 10 nm, while the second undulator is tuned to 2 nm, the fifth harmonic. These undulators are separated by a quadrupole and a 30 cm drift space. This builds on Ref. [10], where the wavelength is tuned to 10 nm. The parameters of the simulation are given in Table III. The first undulator is very short, ending after 5 periods at 28 cm. This increases the bunching at the fifth harmonic from 0.9% to a peak of 2.9%, seeding the beam for its entry into the undulator tuned to the fifth harmonic, which consists of 23 periods with a total length of 1.29 m. This distance was chosen empirically to maximize the bunching factor of the fifth harmonic while reducing the undulator length to deter excessive modulation of the phase space due to space charge effects and increasing the beam energy spread due to the FEL process. Since the source term for the FEL in prebunched FEL operation is proportional to the square of the bunching factor, this increase in bunching is equivalent to an increase in initial bunching equivalent seed power (i.e., lasing at the fundamental) by almost an order of magnitude. The large bunching fraction at the entrance of the second undulator enables lasing at high power in a short undulator. The slippage between the radiation and the electron beam causes the attosecond pulse to lengthen. By radiating at the shorter wavelength, the slippage is reduced resulting in a shorter final pulse.

TABLE III. Simulation parameters for the 2 nm harmonic generation setup. The pulse length is 1 standard deviation. The K values are rms.

Pulse parameters	Value
Photon energy	0.620 keV
Pulse length	41.9 as
Pulse energy	6.85 μJ
Peak power	77.6 GW
Simulation parameters	**Value**
Undulator period	5.60 cm
Harmonic 1 K	3.72
Harmonic 1 number of periods	5
Harmonic 1 photon wavelength	10.00 nm
Harmonic 5 K	1.40
Harmonic 5 number of periods	23
Harmonic 5 photon wavelength	2.00 nm

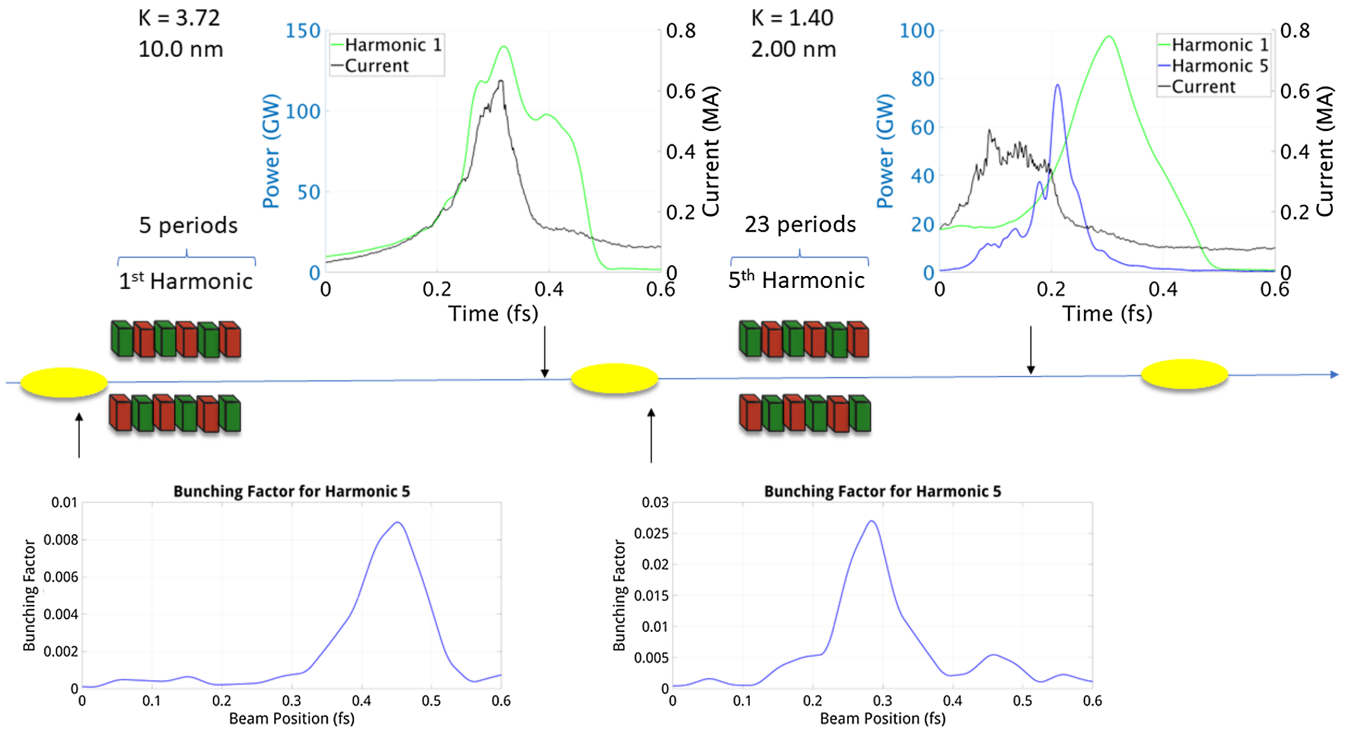

FIG. 2. X-ray power profiles for the fundamental and fifth harmonic along the 2 nm attosecond beamline as well as the bunching factor for the fifth harmonic. This shows how a high-power, attosecond pulse at 2 nm can be produced compactly using coherent harmonic generation and functions as an extension to the TW-scale 10 nm pulse proposed in Ref. [10]. This photon energy extends beyond the C, N, and O K edges, making it useful for various chemical and biological systems [33]. The yellow circle represents the electron beam after it has been generated in a plasma wakefield accelerator (PWFA) and fully compressed traveling down the set of undulators.

The beam dynamics in this multiundulator harmonic generation setup are strongly affected by the LSC forces acting on the beam as it traverses the undulator and drift sections. LSC can be neglected in the limit $L_p \ll L_g$, where L_p is the relativistic plasma wavelength and L_g is the FEL gain length. The relativistic plasma wavelength is given by Eq. (1).

$$L_p = \sqrt{\frac{I_A \gamma \gamma_z^2 \sigma_r^2}{2 I_e}} \tag{1}$$

σ_r is the rms electron beam size, γ is the average Lorentz factor of the beam, γ_z is the average Lorentz factor defined as $\gamma_z = \frac{\gamma}{\sqrt{1+K^2/2}}$, $I_A \approx 17$ kA is the Alfvén current, and I_e is the electron beam peak current [25,31].

Typical XFEL operational parameters satisfy this condition so LSC is usually a perturbation to the beam dynamics. However, the parameters used in this experiment produce L_p and L_g within a factor of 2 of each other, so this assumption is no longer valid. For this reason, we added in space charge effects using the treatment in Ref [32] to the PUFFIN code. We apply the energy modulation due to the longitudinal space charge at each undulator period and each drift section and this contributes to the increase of non-negligible energy chirps on the electron beam as it traverses the undulator. In the case of the 2 nm simulation, the chirp, calculated empirically from simulation, increases in the first undulator at an average rate of 0.511 MeV/nm per period.

The main effect of LSC here is to introduce a positive energy chirp on the beam, lengthening the bunch as it traverses the undulator and reducing the peak current. This effect further underscores the importance of using short undulators in this harmonic-generating plasma-driven XFEL scheme to drive prebunching and x-ray pulse generation before spoiling the beam quality and degrading FEL performance in downstream sections.

Figure 2 shows the longitudinal power profile of the two colors along the beamline in the 2 nm simulation. The Wigner distributions of the pulses are given in Appendix A. The spike in the bunching factor is responsible for the 2 nm pulse produced at the end of this beamline. Along the beamline, as the radiation slips out of the current spike, the region of bunching drifts away from the pulse, which would produce more radiation spikes separated in time. For that reason, the second undulator stage was chosen to cut off before this effect can arise, mitigating the generation of a multicycle pulse and increasing the pulse length. Figure 3 depicts the FWHM of the pulses produced by the setup described in Fig. 2. The final pulse length for the original 10 nm pulse is 166 as, while the 2 nm pulse leaves the beamline with a final pulse length of 41.9 as. Table III summarizes the final photon pulses produced by this scheme. The angular stability of this scheme is discussed in Appendix B.

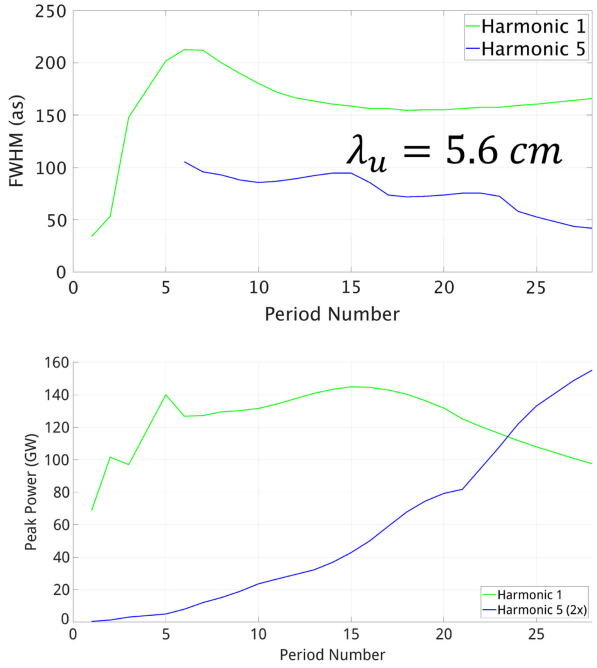

FIG. 3. Pulse length and peak power produced in the 2 nm simulation. The minimum pulse length here is competitive with the shortest HHG pulses ever measured, 43 as [34].

We note that such short pulses are at the limit of what has been achieved to date in terms of minimum pulse duration with high-harmonic generation (HHG) sources [34]. In contrast with HHG sources, the much higher ($\sim 10^6\times$) pulse energy of this attosecond XFEL pulse enables the study of nonlinear processes with sub-100-as resolution as well as the application of two-color attosecond pump-probe techniques due to the multicolor nature of the output.

B. 0.40 nm simulation

The second harmonic generation scheme we consider is a two-stage undulator setup in which the first undulator is tuned to the fundamental at 2 nm while the second undulator is tuned to 0.40 nm. The undulators here are also separated by a quadrupole and 30 cm drift space. These wavelengths were chosen to demonstrate how harmonic generation can be used to produce a 100-as or shorter x-ray pulse at a photon wavelength shorter than possible by conventional means. Other methods to produce GW or TW x-ray pulses using conventional FEL technologies produce pulses significantly longer, over 100-as, pulses [5,35]. The parameters of the undulator are given in Table IV. The first undulator ends after 17 periods at 51 cm, chosen much like the 2 nm simulation to maximize the growth of the fifth harmonic bunching factor and minimize excessive modulation due to space charge. The increase in chirp in the first

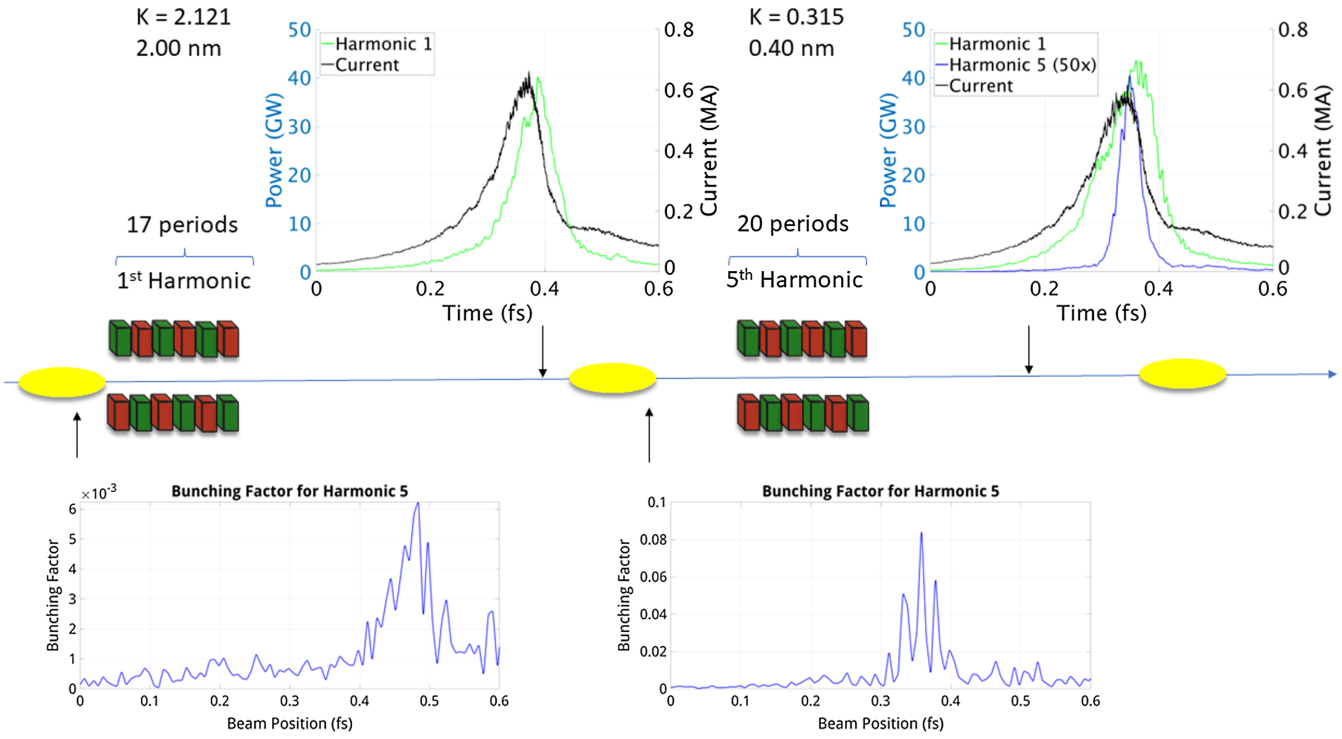

FIG. 4. X-ray power profiles for both the fundamental and fifth harmonic along the two-stage attosecond harmonic-generating beamline tuned to 2 and 0.40 nm, as well as the bunching factor for the fifth harmonic showing an order of magnitude increase before and after the first undulator section.

TABLE IV. Simulation parameters for the 0.4 nm harmonic generation setup. The pulse length is 1 standard deviation. The K values are rms.

Pulse parameters	Value
Photon energy	3.44 keV
Pulse length	40.2 as
Pulse energy	57.6 nJ
Peak power	0.808 GW

Simulation parameters	Value
Undulator period	0.03 m
Harmonic 1 K	2.121
Harmonic 1 number of periods	17
Harmonic 1 photon wavelength	2 nm
Harmonic 5 K	0.315
Harmonic 5 number of periods	20
Harmonic 5 photon wavelength	0.40 nm

undulator is significantly smaller than in the 2 nm simulation, at an average of 0.0921 MeV/nm per period, which is why the effect on the current spike is more pronounced in the 2 nm simulation, whereas the current profile maintains its structure over more periods in the 0.4 nm simulation. Figure 4 shows the longitudinal power profile of each color along the beamline in the two-stage simulation.

The pulse envelope of the fifth harmonic is also delayed by 48 as behind the fundamental and closely resembles the profile of the current spike, further indicating this pulse was produced in the second undulator, utilizing the bunching produced in the first undulator. Additionally, it reaches a high peak power of 0.808 GW. The growth in the bunching factor in Fig. 4 also highlights the utility of this method. The bunching factor grows from a peak of 0.7% to 9%. A larger growth in the bunching factor is seen in this case because space charge limits the growth of the bunching factor in the 2 nm simulation. Figure 5 depicts how this pulse length evolves over the course of the beamline, showing it stabilizes at 40.2 as FWHM. Table IV summarizes the key parameters of the final photon pulse generated and the simulation parameters in the 0.4 nm case.

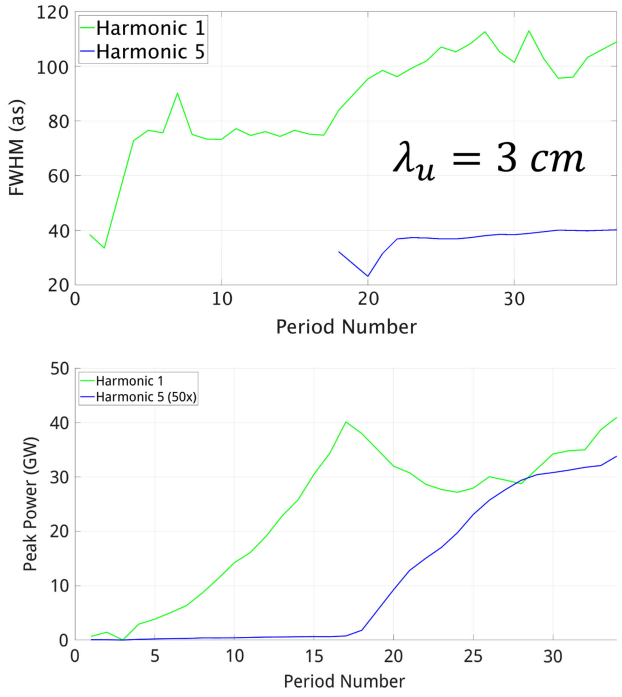

FIG. 5. Pulse length and peak power produced in the 0.40 nm simulation. This demonstrates how the pulse length at the fifth harmonic remains sub-100-as across the entire beamline.

III. CONCLUSION

In this paper, we have presented a method for reaching short sub-nm wavelengths and multicolor operation in a plasma-driven attosecond x-ray source. The scheme exploits harmonic generation in a multiundulator setup to generate high-harmonic bunching and employ retuned undulators to convert the bunching into harmonic radiation. This approach enables a new frontier of attosecond x-ray science through the production of ultrashort (sub-100-as) high-peak power (GW level) pulses with wavelength tunability and at wavelengths as short as 0.40 nm exceeding the carbon K edge, as well as the K edges for most biologically relevant elements. The largest advantage this method has over HGHG is the ability to generate 10s of attosecond pulses while still maintaining GW-scale peak powers. The simulation studies presented have demonstrated the ability to use this technique in two largely interchangeable setups: one to produce two pulses at tens of gigawatts of power and wavelengths at 10 and 2 nm, useful for pump-probe experiments of materials with K edges above 2 nm, and one to produce two as pulses at 2 and 0.4 nm, useful for pump-probe applications where keV-scale photon energies, GW-scale powers, and attosecond pulses are necessary. We note that different undulator tapering strategies can be utilized in conjunction with the harmonic-based approach presented here to, for example, increase the radiation bandwidth, maximize bunching while reducing fundamental output, or maximize photon production in a given section to tailor the pulse properties for particular experiments. Additionally, adding a chicane as a delay between the two undulators can introduce a delay between the two pulses. A delay method using a chicane in this manner has been demonstrated in [36,37]. These manipulations will be investigated in future work.

ACKNOWLEDGMENTS

This work was supported by the U.S. Department of Energy under Contract No. DE-AC02-76SF00515.

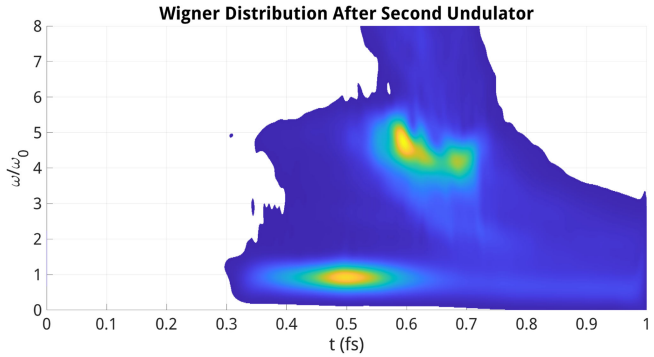

FIG. 6. Wigner distribution of the light produced by this scheme after the second undulator for the 2 nm output case. This highlights the significant bandwidth of the pulse, which may be advantageous for applications requiring high-spectral coherence.

APPENDIX A: PULSE WIGNER DISTRIBUTIONS

Figure 6 depicts the Wigner distribution of the 2 nm simulation after the second undulator. Note the production of the second pulse at the fifth harmonic, trailing the main pulse by 0.1 to 0.2 fs.

Figure 7 also depicts the Wigner distribution after the second undulator but for the 0.4 nm simulation. In this case, the fifth harmonic is significantly fainter, consistent with the fact that the fifth harmonic has a peak power about 50 times less than its fundamental, while the 2 nm simulation had a peak power on the order of its fundamental.

APPENDIX B: ANGULAR STABILITY

To ensure that this effect could be preserved for realistic machine parameters and can be replicated with a realistic jitter, studies of the 2 nm simulation were repeated with the beam offset at various angles. The fifth harmonic bunching factor at the end of the first undulator is depicted as a function of beam position and angular offset in Fig. 8.

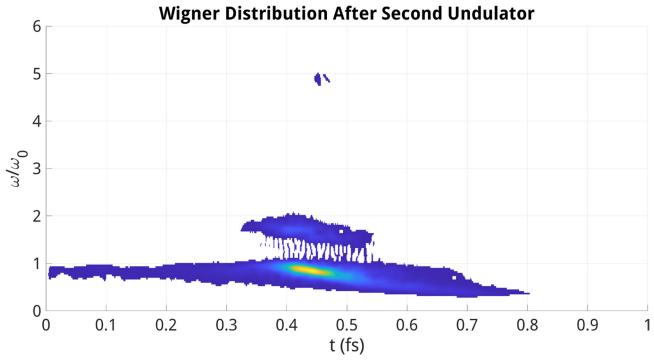

FIG. 7. Wigner distribution of the light produced by this scheme after the second undulator for the 0.4 nm output case.

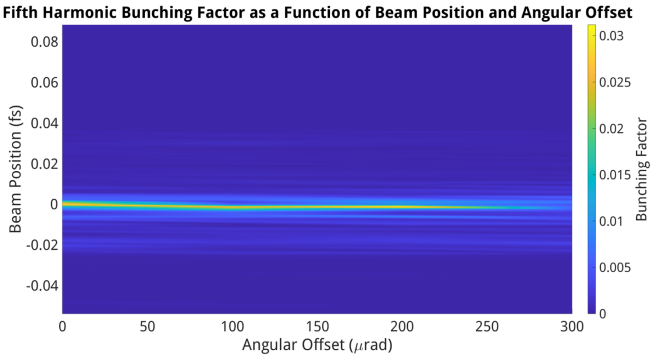

FIG. 8. The fifth harmonic bunching factor as a function of beam position and angular offset at the end of the first undulator in the 2 nm simulation.

The peak bunching factor begins to fall off significantly after an angular offset of approximately 200 μrad, consistent with what was simulated in [10].

[1] C. Pellegrini, A. Marinelli, and S. Reiche, The physics of x-ray free-electron lasers, Rev. Mod. Phys. **88**, 015006 (2016).

[2] J. Duris *et al.*, Tunable isolated attosecond x-ray pulses with gigawatt peak power from a free-electron laser, Nat. Photonics **14**, 30 (2020).

[3] J. P. Duris *et al.*, Controllable x-ray pulse trains from enhanced self-amplified spontaneous emission, Phys. Rev. Lett. **126**, 104802 (2021).

[4] Z. Zhang, J. Duris, J. P. MacArthur, A. Zholents, Z. Huang, and A. Marinelli, Experimental demonstration of enhanced self-amplified spontaneous emission by photocathode temporal shaping and self-compression in a magnetic wiggler, New J. Phys. **22**, 083030 (2020).

[5] S. Huang, Y. Ding, Y. Feng, E. Hemsing, Z. Huang, J. Krzywinski, A. Lutman, A. Marinelli, T. Maxwell, and D. Zhu, Generating single-spike hard x-ray pulses with nonlinear bunch compression in free-electron lasers, Phys. Rev. Lett. **119**, 154801 (2017).

[6] A. Marinelli, J. MacArthur, P. Emma, M. Guetg, C. Field, D. Kharakh, A. Lutman, Y. Ding, and Z. Huang, Experimental demonstration of a single-spike hard-x-ray free-electron laser starting from noise, Appl. Phys. Lett. **111**, 151101 (2017).

[7] A. Malyzhenkov, Y. P. Arbelo, P. Craievich, P. Dijkstal, E. Ferrari, S. Reiche, T. Schietinger, P. Juranić, and E. Prat, Single- and two-color attosecond hard x-ray free-electron laser pulses with nonlinear compression, Phys. Rev. Res. **2**, 042018 (2020).

[8] F. Krausz and M. Ivanov, Attosecond physics, Rev. Mod. Phys. **81**, 163 (2009).

[9] J. Breidbach and L. S. Cederbaum, Universal attosecond response to the removal of an electron, Phys. Rev. Lett. **94**, 033901 (2005).

[10] C. Emma, X. Xu, A. Fisher, R. Robles, J. P. MacArthur, J. Cryan, M. J. Hogan, P. Musumeci, G. White, and

A. Marinelli, Terawatt attosecond x-ray source driven by a plasma accelerator, APL Photonics **6**, 076107 (2021).

[11] C. Emma, Status and prospects for the Plasma-Driven Attosecond X-Ray (PAX) experiment at Facet-II, in *Proceedings of the 13th International Particle Accelerator Conference, IPAC-2022, Bangkok, Thailand* (JACoW, Geneva, Switzerland, 2022).

[12] R. Hessami, Multicolor operation via coherent harmonic generation in a plasma driven attosecond x-ray source, in *Proceedings of the 14th International Particle Accelerator Conference, Venice, Italy* (JACoW, Geneva, Switzerland, 2023).

[13] R. Robles, C. Emma, R. Hessami, K. Larsen, and A. Marinelli, Generating sub-femtosecond electron beams at plasma wakefield accelerators, in *Proceedings of the 13th International Particle Accelerator Conference, IPAC-2022, Bangkok, Thailand* (JACoW, Geneva, Switzerland, 2022).

[14] L. H. Yu, M. Babzien, I. Ben-Zvi, L. F. DiMauro, A. Doyuran, W. Graves, E. Johnson, S. Krinsky, R. Malone, I. Pogorelsky, J. Skaritka, G. Rakowsky, L. Solomon, X. J. Wang, M. Woodle, V. Yakimenko, S. G. Biedron, J. N. Galayda, E. Gluskin, J. Jagger, V. Sajaev, and I. Vasserman, High-gain harmonic-generation free-electron laser, Science **289**, 932 (2000).

[15] E. Allaria, R. Appio, L. Badano, W. Barletta, S. Bassanese, S. Biedron, A. Borga, E. Busetto, D. Castronovo, P. Cinquegrana *et al.*, Highly coherent and stable pulses from the fermi seeded free-electron laser in the extreme ultraviolet, Nat. Photonics **6**, 699 (2012).

[16] E. Allaria, D. Castronovo, P. Cinquegrana, P. Craievich, M. Dal Forno, M. Danailov, G. D'Auria, A. Demidovich, G. De Ninno, S. Di Mitri *et al.*, Two-stage seeded soft-x-ray free-electron laser, Nat. Photonics **7**, 913 (2013).

[17] G. Stupakov, Using the beam-echo effect for generation of short-wavelength radiation, Phys. Rev. Lett. **102**, 074801 (2009).

[18] D. Xiang, E. Colby, M. Dunning, S. Gilevich, C. Hast, K. Jobe, D. McCormick, J. Nelson, T. Raubenheimer, K. Soong *et al.*, Evidence of high harmonics from echo-enabled harmonic generation for seeding x-ray free electron lasers, Phys. Rev. Lett. **108**, 024802 (2012).

[19] E. Hemsing, M. Dunning, B. Garcia, C. Hast, T. Raubenheimer, G. Stupakov, and D. Xiang, Echo-enabled harmonics up to the 75th order from precisely tailored electron beams, Nat. Photonics **10**, 512 (2016).

[20] P. Rebernik Ribič, A. Abrami, L. Badano, M. Bossi, H.-H. Braun, N. Bruchon, F. Capotondi, D. Castronovo, M. Cautero, P. Cinquegrana *et al.*, Coherent soft x-ray pulses from an echo-enabled harmonic generation free-electron laser, Nat. Photonics **13**, 555 (2019).

[21] A. F. Habib, G. G. Manahan, P. Scherkl, T. Heinemann, A. Sutherland, R. Altuiri, B. M. Alotaibi, M. Litos, J. Cary, T. Raubenheimer, E. Hemsing, M. J. Hogan, J. B. Rosenzweig, P. H. Williams, B. W. McNeil, and B. Hidding, Attosecond-Angstrom free-electron-laser towards the cold beam limit, Nat. Commun. **14**, 1054 (2023).

[22] Y. Xiao, C. Feng, and B. Liu, Generating isolated attosecond x-ray pulses by wavefront control in a seeded free-electron laser, Ultrafast Sci. **2022**, 9812478 (2022).

[23] R. Bonifacio, C. Pellegrini, and L. Narducci, Collective instabilities and high-gain regime in a free electron laser, Opt. Commun. **50**, 373 (1984).

[24] K.-J. Kim, Z. Huang, and R. Lindberg, *Synchrotron Radiation and Free-Electron Lasers* (Cambridge University Press, Cambridge, England, 2017).

[25] J. B. Rosenzweig, *Fundamentals of Beam Physics* (Oxford University Press, New York, 2003).

[26] A. A. Zholents, Method of an enhanced self-amplified spontaneous emission for x-ray free electron lasers, Phys. Rev. ST Accel. Beams **8**, 040701 (2005).

[27] Y. Ding, Z. Huang, D. Ratner, P. Bucksbaum, and H. Merdji, Generation of attosecond x-ray pulses with a multicycle two-color enhanced self-amplified spontaneous emission scheme, Phys. Rev. ST Accel. Beams **12**, 060703 (2009).

[28] P. Baxevanis, J. Duris, Z. Huang, and A. Marinelli, Time-domain analysis of attosecond pulse generation in an x-ray free-electron laser, Phys. Rev. Accel. Beams **21**, 110702 (2018).

[29] L. T. Campbell and B. W. McNeil, Puffin: A three dimensional, unaveraged free electron laser simulation code, Phys. Plasmas **19**, 093119 (2012).

[30] D. A. Jaroszynski, R. J. Bakker, A. F. Van Der Meer, D. Oepts, and P. W. Van Amersfoort, Coherent startup of an infrared free-electron laser, Phys. Rev. Lett. **71**, 3798 (1993).

[31] G. Marcus, E. Hemsing, and J. Rosenzweig, Gain length fitting formula for free-electron lasers with strong space-charge effects, Phys. Rev. ST Accel. Beams **14**, 080702 (2011).

[32] G. Geloni, E. Saldin, E. Schneidmiller, and M. Yurkov, Longitudinal impedance and wake from XFEL undulators. Impact on current-enhanced SASE schemes, Nucl. Instrum. Methods Phys. Res., Sect. A **583**, 228 (2007).

[33] D. Attwood, *Soft X-Rays and Extreme Ultraviolet Radiation* (Cambridge University Press, Cambridge, England, 1999).

[34] T. Gaumnitz, A. Jain, Y. Pertot, M. Huppert, I. Jordan, F. Ardana-Lamas, and H. J. Wörner, Streaking of 43-attosecond soft-x-ray pulses generated by a passively CEP-stable mid-infrared driver, Opt. Express **25**, 27506 (2017).

[35] E. Prat, A. Malyzhenkov, C. Arrell, P. Craievich, S. Reiche, T. Schietinger, and G. Wang, Coherent sub-femtosecond soft x-ray free-electron laser pulses with nonlinear compression, APL Photonics **8**, 111302 (2023).

[36] Z. Guo *et al.*, Experimental demonstration of attosecond pump–probe spectroscopy with an x-ray free-electron laser, Nat. Photonics **18**, 691 (2024).

[37] S. Li, L. Lu, S. Bhattacharyya, C. Pearce, K. Li, E. T. Nienhuis, G. Doumy, R. D. Schaller, S. Moeller, M.-F. Lin, G. Dakovski, D. J. Hoffman, D. Garratt, K. A. Larsen, J. D. Koralek, C. Y. Hampton, D. Cesar, J. Duris, Z. Zhang, N. Sudar, J. P. Cryan, A. Marinelli, X. Li, L. Inhester, R. Santra, and L. Young, Attosecond-pump attosecond-probe x-ray spectroscopy of liquid water, Science **383**, 1118 (2024).